Datasheet-based Loss Model of a GaN-Based Single-Stage Standalone Lighting System

Renan R. Duarte, *Student Member, IEEE,* Nelson S. Spode, Lucas Teixeira, *Member, IEEE*
J. Marcos Alonso, *Senior Member, IEEE* and Marco A. Dalla Costa, *Senior Member, IEEE*

I. System Topology

During daytime, the circuit behaves as a synchronous buck converter (Fig. 1a), harvesting energy from the solar panel and storing it in the battery. At night, it acts as a synchronous boost converter (Fig. 1b), supplying the LED from the battery.

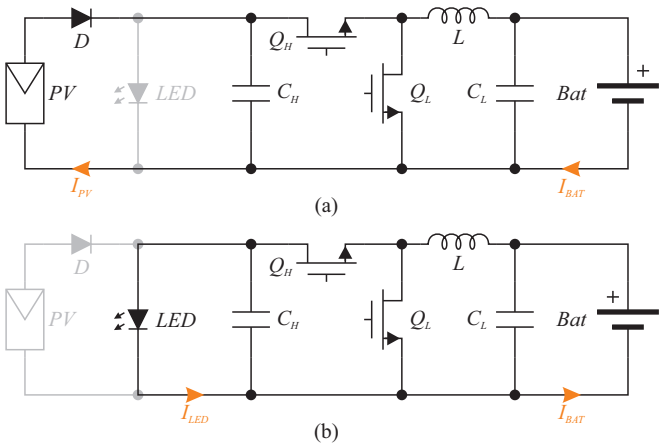

Fig. 1. Equivalent circuit of the converter during the day - charging mode (a) and during the night - driver mode (b).

II. Loss Model

Power losses in a switching converter can be divided into three major categories: passives (power inductor and capacitors), actives (e.g., conduction and switching losses in the power semiconductors) and others (e.g., gate drivers, sensing elements, voltage regulators, etc.). Each of these groups will be further analyzed in the following subsections. This analysis considers a converter operating under continuous conduction mode (CCM).

A. Passive Components

In the bidirectional converter under analysis, the losses due to passive components in the power loop are concentrated mainly in the power inductor L. As demonstrated by previous works with similar topologies, losses in the power capacitors C_H and C_L account for a very small portion of the overall losses, so they can be neglected to simplify the model [1]–[3].

Losses in the power inductor can be further expanded in core and winding losses. The former can be estimated using different methods proposed over the years. These models differ from each other both in terms of precision and complexity [4]. If extreme precision is required, usually an experimental characterization of the inductor is needed.

However, to speed-up the design process, a methodology that relies only on data known beforehand is desired. The Modified Steinmetz Equation (MSE) method expands the classical Steinmetz Equation for non-sinusoidal excitation and can be used to estimate the inductor core losses with enough precision using only parameters found in the datasheet of the device [5]. Using this method, the core losses are given by

$$P_{L_{core}} = K \cdot {f_{sin_{eq}}}^{(\alpha-1)} \cdot {B_{pk}}^{\beta} \cdot f_{sw}, \tag{1}$$

where α and β are the Steinmetz coefficients, K is the volume constant, B_{pk} is the peak magnetic flux density, f_{sw} is the switching frequency and $f_{sin_{eq}}$ is the equivalent sinusoidal frequency. For an inductor under squarewave voltage excitation, the equivalent frequency is dependent on the duty cycle D of the waveform, as in (2).

$$f_{sin_{eq}} = \frac{2}{\pi^2} \frac{f_{sw}}{D - D^2} \tag{2}$$

Winding losses, on the other hand, can be modeled by dividing the losses into its DC and AC components. The former is caused mainly by the parasitic DC resistance of the conductor and can be determined by

$$P_{L_{DC}} = {I_{L_{DC}}}^2 \cdot R_{DC}(T), \tag{3}$$

where $I_{L_{DC}}$ is the average current in the inductor and $R_{DC}(T)$ is the DC winding resistance. This resistance increases as the inductor temperature rises. To improve the model accuracy, this effect can be modeled using (4), where $R_{DC_{nom}}$ is the nominal resistance (typically defined at 25°C), k_{temp} is the device's temperature coefficient and ΔT is the temperature deviation from the nominal value.

$$R_{DC}(T) = R_{DC_{nom}} \cdot k_{temp} \cdot \Delta T, \tag{4}$$

AC losses are related to the skin and proximity effects that lead to eddy currents in the winding conductors, which increase losses under high current and high frequency conditions. To fully characterize these components, knowledge about the physical construction of the device is required (e.g., number of turns, geometry of the conductor, etc.) [2]. However, in many cases this data is not known, especially with commercially available inductors.

To overcome this limitation, manufacturers usually provide an equivalent AC resistance R_{AC}. Using this parameter and

the RMS current of the inductor $I_{L_{RMS}}$, these losses can be approximated with sufficient precision as in (5) [6].

$$P_{L_{AC}} = {I_{L_{RMS}}}^2 \cdot R_{AC}(T) \tag{5}$$

The effects of temperature changes in the AC resistance $R_{AC}(T)$ can also be estimated as in (4).

By combining (1), (3) and (5), one can obtain the estimated losses in the inductor:

$$P_L = P_{L_{core}} + P_{L_{DC}} + P_{L_{AC}} \tag{6}$$

B. Active Components

Active components' losses comprehend the conduction and switching losses in the power semiconductors. Depending on the operating mode of the converter, the switches Q_H and Q_L alternate between main and free-wheeling device. Given this reason, in the after-mentioned equations, a generic switch Q is considered. This device can be Q_H or Q_L depending on the mode.

Conduction losses are relatively easy to estimate. Similar to Si-based devices, for GaN HEMTs they are defined as

$$P_{Q_{cond}} = {I_{Q_{RMS}}}^2 \cdot R_{DSon}, \tag{7}$$

where $I_{Q_{RMS}}$ is the RMS current through the device and R_{DSon} is the switch on-state resistance.

In the free-wheeling device, conduction losses are further divided into two elements. The first one occurs while the device is kept active by the gate signal and is estimated using (7). The second occurs during the dead-time (DT) when the current flows through the intrinsic body diode of the switch (despite not having a true body diode like Si MOSFETs, GaN-based devices have similar behavior when reverse polarized [7]). In this interval, conduction losses are determined by

$$P_{Q_{DT}} = I_{Q_{DT}} \cdot V_{Q_{SD}}, \tag{8}$$

where $I_{Q_{dt}}$ is the average switch current during this interval and $V_{Q_{SD}}$ is the switch voltage drop when reverse polarized.

Same as with the inductor, variations in junction temperature also affect the parasitic resistances of the semiconductor. These deviations can also be modeled using (4).

Switching losses, on the other hand, are tricky to estimate due to the parasitic elements present in the real circuit and non-linearities in devices' parameters. Many past works focused on modeling parasitic elements and evaluating switching losses [8], [9]. This approach, however, usually results in complex models which are extremely application-dependent. Simple loss models are desirable as they reduce the overall complexity of the system speeding up the design process [10].

If some degree of uncertainty is acceptable, the estimation of the switching losses can be simplified by dividing them into three different elements, as shown in (9).

$$P_{Q_{sw}} = P_{Q_{Cout}} + P_{Q_{on}} + P_{Q_{off}} \tag{9}$$

In this equation, $P_{Q_{Cout}}$ is the loss related to the energy stored in the drain-to-source capacitance of the switch that is discharged in each switching cycle. $P_{Q_{on}}$ and $P_{Q_{off}}$ are the turn-on and turn-off losses, respectively.

The first element is defined by

$$P_{Q_{Cout}} = \frac{1}{2}\left(Q_{Coss} - Q_{Crss}\right) \cdot {V_{DS}}^2 \cdot f_{sw}, \tag{10}$$

where Q_{Coss} and Q_{Crss} are the output and reverse capacitances of the device and V_{DS} is the drain-to-source voltage over the switch.

At the main switch, turn-on and turn-off transitions occur when the inductor current is at its extreme values, resulting in losses due to the overlap of device's voltage and current during these intervals, as shown in Fig. 2 [7]. Transition losses can be approximated by (11) and (12) [7], in which $I_{L_{min}}$ and $I_{L_{max}}$ are the inductor currents at the transition instants and $t_{Q_{on}}$ and $t_{Q_{off}}$ are the interval durations. These timing parameters are dependent on the gate driver circuitry used (e.g., gate resistor values, source and sink currents, etc.).

$$P_{Q_{on}} = \frac{1}{2} V_{DS} \cdot I_{L_{min}} \cdot t_{Q_{on}} \cdot f_{sw} \tag{11}$$

$$P_{Q_{off}} = \frac{1}{2} V_{DS} \cdot I_{L_{max}} \cdot t_{Q_{off}} \cdot f_{sw} \tag{12}$$

In the free-wheeling switch, turn-on and turn-off transitions occur when the current is flowing through the body diode, giving the circuit a characteristic similar to soft-switching in this device [10], [11]. Furthermore, unlike silicon MOSFETs, GaN devices present no reverse recovery effect. Hence, in this analysis, losses related to these transitions are considered negligible.

By combining (7), (8) and (9), one can obtain the estimated losses in one switch:

$$P_Q = P_{Q_{cond}} + P_{Q_{dt}} + P_{Q_{sw}} \tag{13}$$

C. Other Components

Other miscellaneous losses include gate driver losses (the energy spent to turn both switches on and off) and losses in the auxiliary circuits such as sensors and the control circuitry, as in (14).

$$P_{other} = P_{driver} + P_{aux} \tag{14}$$

Gate driver losses depend both on the specific circuitry used and the switching frequency [7]. On the other hand, losses in

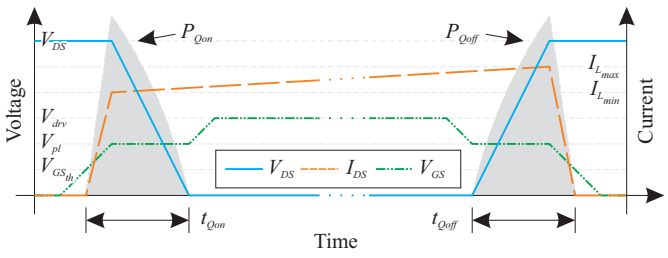

Fig. 2. Voltage and current waveforms at the main switch during turn-on and turn-off transitions. Axis not to scale.

the auxiliary circuits are usually independent of the switching frequency and power levels. So, it is common practice to consider them constant over the entire operating range of the converter [12], [13]. Despite being small compared to the rated power of the converter, these losses become more pronounced in the overall efficiency of the converter in light-load scenarios [14]. Given this reason, it is important to account for these losses.

D. Model Validation

Before using the presented model in the optimization procedure, it needs validation to assert its coherence and accuracy.

The efficiency results of the prototype presented in [15] were compared to the theoretical values estimated using the proposed model. This converter operates with a maximum input power of 100 W in both modes. Two different switching frequencies were analyzed: 250 kHz and 345 kHz.

We estimated operating temperatures in the components using the I_{DC} vs. ΔT plots from the datasheets and the values were used to adjust parameters such as parasitic resistances of components in the model. Effects observed in [15], such as the cross-heating between switches and inductor were ignored. Gate driving losses were estimated considering the IC used (LM5113 by National Semiconductor) and the power consumption of the microcontroller, current sensors and auxiliary power supply were also taken into consideration.

The efficiency in each operating mode was estimated using (15), where P_{in} is the input power of the converter at the considered operation point.

$$\eta_{est} = 1 - \frac{P_L + P_{Q_H} + P_{Q_L} + P_{other}}{P_{in}} \qquad (15)$$

Fig. 3a shows the efficiency curves for the converter operating as a battery charger at 250kHz, while Fig. 3b shows as LED driver at 345kHz. In Table I, the average and maximum error between the experimental and estimated data are presented. Results are analyzed only in the 10-100 W range given the fact that with lighter loads, the converter operates under DCM and the loss model is no longer valid.

As seen, the loss model matches fairly well with the experimental data, especially in the mid- to high-load range. Moreover, the model has relatively small estimation errors in the analyzed power range.

The distribution of losses among the components of the converter at 100W is shown in Fig. 4a for the charger at 250kHz and in Fig. 4b for the driver at 345kHz. As can be seen, in driver mode, both switches present higher losses than in charger mode. This is However, in both modes, the inductor is responsible for the majority of the losses in the circuit.

TABLE I
MODEL EFFICIENCY DEVIATION

Frequency (kHz)	Charger		Driver	
	Avg (%)	Max (%)	Avg (%)	Max (%)
250	0.625	1.63	1.05	1.86
345	0.957	1.29	0.455	2.73

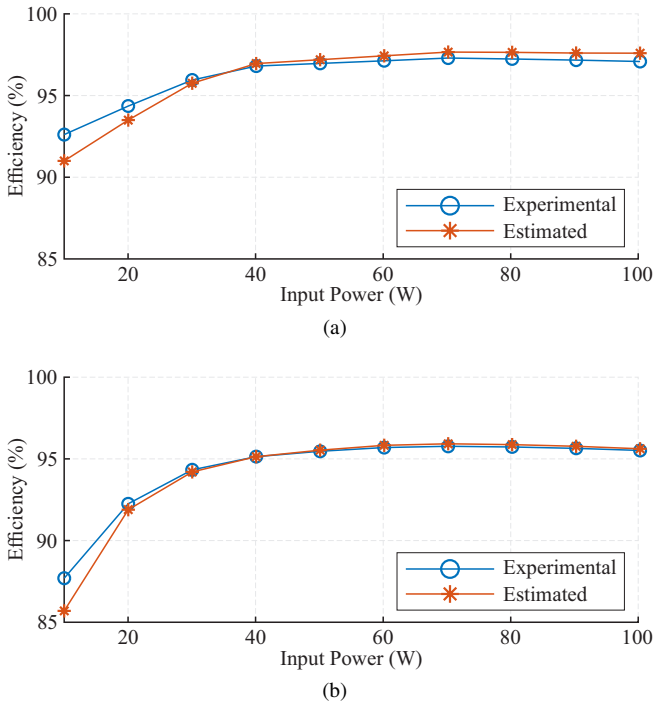

Fig. 3. Measured and estimated efficiencies at different input powers of the 100 W nominal prototype in charger (a) and driver (b) modes.

This further highlights the importance of improving passive components performance as more advanced semiconductor technologies reach the market and allow for higher frequency converters.

REFERENCES

[1] S. Vighetti, J.-P. Ferrieux, and Y. Lembeye, "Optimization and Design of a Cascaded DC/DC Converter Devoted to Grid-Connected Photovoltaic Systems," *IEEE Transactions on Power Electronics*, vol. 27, pp. 2018–2027, apr 2012.

[2] S. Waffler, M. Preindl, and J. W. Kolar, "Multi-objective optimization and comparative evaluation of Si soft-switched and SiC hard-switched automotive DC-DC converters," in *Industrial Electronics Conference (IECON)*, (Porto), pp. 3814–3821, IEEE, 2009.

[3] R. R. Duarte, G. F. Ferreira, M. A. Dalla Costa, and J. M. Alonso, "Performance comparison of Si and GaN transistors in a family of synchronous buck converters for LED lighting applications," in *IEEE Industry Applications Society Annual Meeting*, (Portland), pp. 1–7, IEEE, oct 2016.

[4] K. Venkatachalam, C. R. Sullivan, T. Abdallah, and H. Tacca, "Accurate prediction of ferrite core loss with nonsinusoidal waveforms using only Steinmetz parameters," in *IEEE Workshop on Computers in Power Electronics*, (Mayaguez), pp. 36–41, IEEE, 2002.

[5] M. Albach, T. Durbaum, and A. Brockmeyer, "Calculating core losses in transformers for arbitrary magnetizing currents a comparison of different approaches," in *Annual IEEE Power Electronics Specialists Conference (PESC)*, vol. 2, (Baveno), pp. 1463–1468 vol.2, IEEE, 1996.

[6] M. C. Mira, A. Knott, and M. A. E. Andersen, "Loss distribution analysis of a three-port converter for low-power stand-alone light-to-light systems," in *2016 18th European Conference on Power Electronics and Applications, EPE 2016 ECCE Europe*, (Karlsruhe), pp. 1–10, IEEE, 2016.

[7] A. Lidow, J. Strydom, M. de Rooij, and D. Reusch, *GaN Transistors for Efficient Power Conversion*. Chichester: John Wiley & Sons Ltd, 2 ed., jul 2014.

[8] M. Orabi and A. Shawky, "Proposed switching losses model for integrated point-of-load synchronous buck converters," *IEEE Transactions on Power Electronics*, vol. 30, no. 9, pp. 5136–5150, 2015.

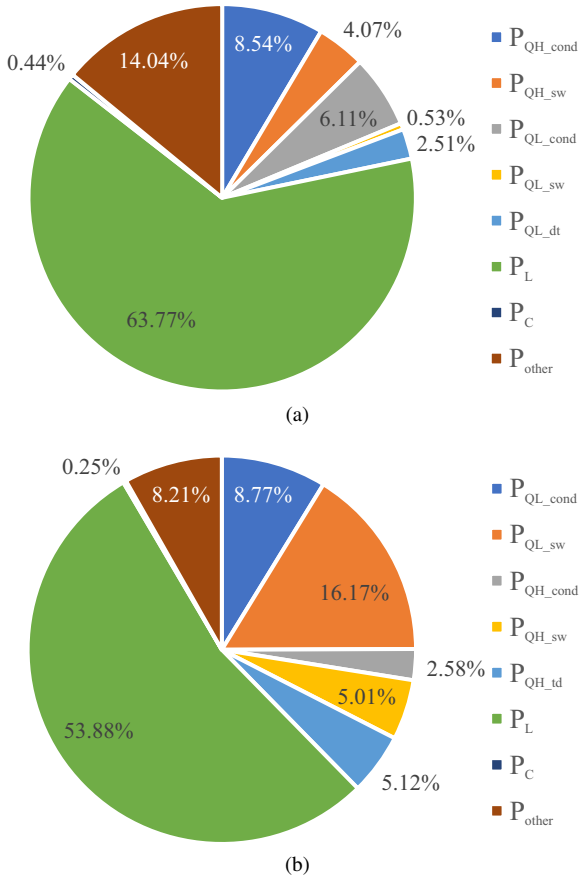

Fig. 4. Estimated loss distribution of the prototype at 100 W in charger (a) and driver (b) modes.

[9] W. Kangping, Y. Xu, Z. Xiangjun, Y. Xiaoling, L. Hongchang, G. Yixuan, G. Bing, and M. Huan, "Analytical loss model of low voltage enhancement mode GaN HEMTs," in *IEEE Energy Conversion Congress and Exposition (ECCE)*, (Pittsburgh), pp. 100–105, IEEE, sep 2014.

[10] Ruiyang Yu, B. M. H. Pong, B. W.-k. Ling, and J. Lam, "Two-Stage Optimization Method for Efficient Power Converter Design Including Light Load Operation," *IEEE Transactions on Power Electronics*, vol. 27, pp. 1327–1337, mar 2012.

[11] K. Kruse, M. Elbo, and Z. Zhang, "GaN-based high efficiency bidirectional DC-DC converter with 10 MHz switching frequency," in *IEEE Applied Power Electronics Conference and Exposition (APEC)*, (Tampa), pp. 273–278, IEEE, mar 2017.

[12] J. W. Kolar, J. Biela, and J. Minibock, "Exploring the pareto front of multi-objective single-phase PFC rectifier design optimization - 99.2% efficiency vs. 7kW/dm3 power density," in *2009 IEEE 6th International Power Electronics and Motion Control Conference*, (Wuhan), pp. 1–21, IEEE, 2009.

[13] F. Jauch and J. Biela, "Generalized modeling and optimization of a bidirectional dual active bridge DC-DC converter including frequency variation," in *International Power Electronics Conference (IPEC - ECCE ASIA)*, (Hiroshima), pp. 1788–1795, IEEE, 2014.

[14] R. R. Duarte, G. G. Pereira, M. A. Dalla Costa, C. H. Barriquello, and J. Marcos Alonso, "Off-grid commercial LED driver optimization using GaN transistors," in *IEEE Industry Applications Society Annual Meeting (IAS)*, (Portland), pp. 1–7, IEEE, 2018.

[15] R. R. Duarte, A. Campos, M. A. Dalla Costa, V. C. Bender, and J. M. Alonso, "Single-Stage Standalone Lighting System Based on GaN Transistors," in *IEEE Industry Applications Society Annual Meeting (IAS)*, (Portland), pp. 1–6, IEEE, 2019.